Investigation of combined effects of cross section, taper angle and cell structure on crashworthiness of multi-cell thin-walled tubes

Murat Altin, Ümit Kılınçkaya, Erdem Acar & Mehmet Ali Güler

Taylor & Francis
Taylor & Francis Group

Check for updates

Investigation of combined effects of cross section, taper angle and cell structure on crashworthiness of multi-cell thin-walled tubes

Murat Altin[a], Ümit Kılınçkaya[b], Erdem Acar[b] and Mehmet Ali Güler [b]

[a]Department of Automotive Engineering, Faculty of Technology, Gazi University, Teknik Okullar, Ankara, Turkey; [b]Department of Mechanical Engineering, TOBB University of Economics and Technology, Ankara, Turkey

ABSTRACT

Crash box design has a substantial importance to reduce the fatalities in a frontal crash. In this study, four different types of multi-cell tubes, namely straight-circular, straight-square, tapered-circular and tapered-square geometries, are considered as energy absorbing components. For each type, seven different cell structures are designed, and the crashworthiness of these designs is assessed based on two different metrics: crush force efficiency (CFE) and specific energy absorption (SEA). When the thickness and the taper angle are fixed, the multi-cell design having the best performance is found to have 165% larger CFE and 237% larger SEA compared to the single-cell design having the worst performance. By varying the thickness, the CFE and SEA performances of the best design can be further increased by 5% and 7%, respectively. Similarly, by varying the taper angle, the SEA performances of the best design with varied thickness can further be increased by 4%.

HIGHLIGHTS

- Impact behaviour of several multi-cell straight and tapered tubes are investigated
- All multi-cell models have larger CFE and SEA values than the single-cell models
- Tapered-circular tube has the best, straight-square has the worst crush performance
- CFE of the best multi-cell design is 177% larger than the worst single-cell design
- SEA of the best multi-cell design is 275% larger than the worst single-cell design

1. Introduction

Automakers aim to produce lighter vehicles to decrease the brake specific fuel consumption without jeopardising the passenger and vehicle safety. Energy absorbers located in the front bumper of the road vehicles have the capability of absorbing energy by deforming plastically in case of a frontal collision crash, thereby reducing the axial force transferred directly to the passenger cabin and improving the safety [1,2].

Thin-walled structures are often used as energy absorbers. These structures can have single-cell or multi-cell structure, and it has been shown that the multi-cell structures have better crush performance compared to the single-cell structures [3,4]. In the literature, the effects of various parameters such as cross-sectional shape, taper angle, thickness and cell structure on crashworthiness of multi-cell thin-walled tubes are investigated. However, the existing studies in the literature focus on the individual effects of these parameters as can be seen in a recent review article [5], and the literature lacks the investigation of the interactions and combined effects of these parameters.

Although there are several articles related to the crashworthiness of thin-walled structures, herein we review the articles most relevant to our study. The effects of the cross-sectional shape on the crush performance of the multi-cell tubes were explored by the authors in [6–12]. It was found that the octagonal and hexagonal cross sections are favourable over other cross sections. The effects of taper angle on crashworthiness of single-cell or multi-cell rectangular thin-walled tubes were investigated by the authors in [13–19], whereas the effect of tapering on circular profiles has not been investigated yet. It was observed that as the taper angle was increased, the energy absorption capacity of the tubes was also increased. The effect of the cell structure on crashing capability of the multi-cell tubes were explored by the authors in [6,15,16,20]. It was found that as the number of cells was increased, the energy abruption capability of the multi-cell tubes was also increased. It was also found that circular cross section had better crush performance for bitubal multi-cell tubes, whereas hexagonal and octagonal sections had better crush performance for

---

other multi-cell tubes. For the state of the art and recent advances on crashworthiness of thin-walled energy absorbers, the readers are referred to the review articles [5,21].

As noted earlier, the existing literature focus mostly on individual effects of cross section, taper angle and cell structure on crashworthiness of multi-cell thin-walled tubes, whereas the investigation of interactions and combined effects of these parameters is missing in the literature, and this paper aims to fill this gap. It should also be noted that the effect of tapering on multi-cell circular thin-walled tubes has not been investigated yet in the open literature, and this paper presents a novel contribution in this subject. This paper presents a numerical study, where explicit dynamic finite element analysis (FEA) are performed by using LS-DYNA to simulate the crash behaviour of thin-walled tubes under axial impact loading.

The paper is organised as follows. Section 2 presents the key crashworthiness and design parameters for an efficient energy absorber design. Section 3 provides details of FEA. Section 4 compares FEA results with experimental and numerical work in the literature. The results obtained from this study and corresponding discussions are given in Section 5, followed by the concluding remarks presented in Section 6.

2. Energy absorber design

The capability of an energy absorber in dissipating the impact energy depends on its ability to deform plastically before fracture. The crushing capability and energy absorption capacity of an energy absorber can be evaluated with various metrics derived from the load-displacement curve obtained from dynamic axial crushing of energy absorbers [22]. Commonly used crashworthiness metrics are described in the following.

2.1. Total energy absorption

Total absorbed energy is computed from the area under the load-displacement curve. Therefore, the total energy absorbed (EA) is calculated from

$$EA = \int_0^{\delta_c} P \, d\delta \qquad (1)$$

where P is the crush force in axial direction, and δ_c is the cut-off displacement. The energy absorbers change the kinetic energy to other form of energy through deformation.

2.2. Peak crush force

Peak crush force is the force at which first fold starts. The first peak at the load-displacement curve is used to determine the peak crush force.

2.3. Mean crush force

The mean crush force, F_m, is obtained by dividing the total energy absorbed energy, EA, by the cut-off deformation, δ_c. That is, the mean crush force is computed from

$$F_m = \frac{EA}{\delta_c} \qquad (2)$$

2.4. Crush force efficiency (CFE)

The crush force efficiency, CFE, is the ratio of the mean crushing force to the peak crush force (F_p). That is, CFE is calculated from

$$CFE = \frac{F_m}{F_p} \qquad (3)$$

2.5. Specific energy absorption (SEA)

The specific energy absorption, SEA, is defined as the absorbed energy per unit mass. That is, SEA is computed from

$$SEA = \frac{EA}{m} \qquad (4)$$

where m is the mass of the structure.

2.6. Design parameters

In the event of a crash, the peak force is critical to the passenger survival rate when impact occurs. Very high peak force often leads to severe injury or even death of occupant. In crashworthiness design the energy-absorption capacity of a tube is measured by SEA and CFE. Therefore, the major objective of this study is to maximise the SEA and CFE for the straight and tapered tubes. In this study, energy absorption characteristics of four different types of cross-sectional geometry (straight-square, straight-circular, tapered-square and tapered-circular) are evaluated and compared to each other. The geometries of the four different types of energy absorbers are shown in Figure 1. It was found that the length, wall thickness and taper angles of the crash boxes used on passenger cars are between 150 and 220 mm, 1.5 and 3 mm and 0° and 7.5°, respectively. Therefore, design
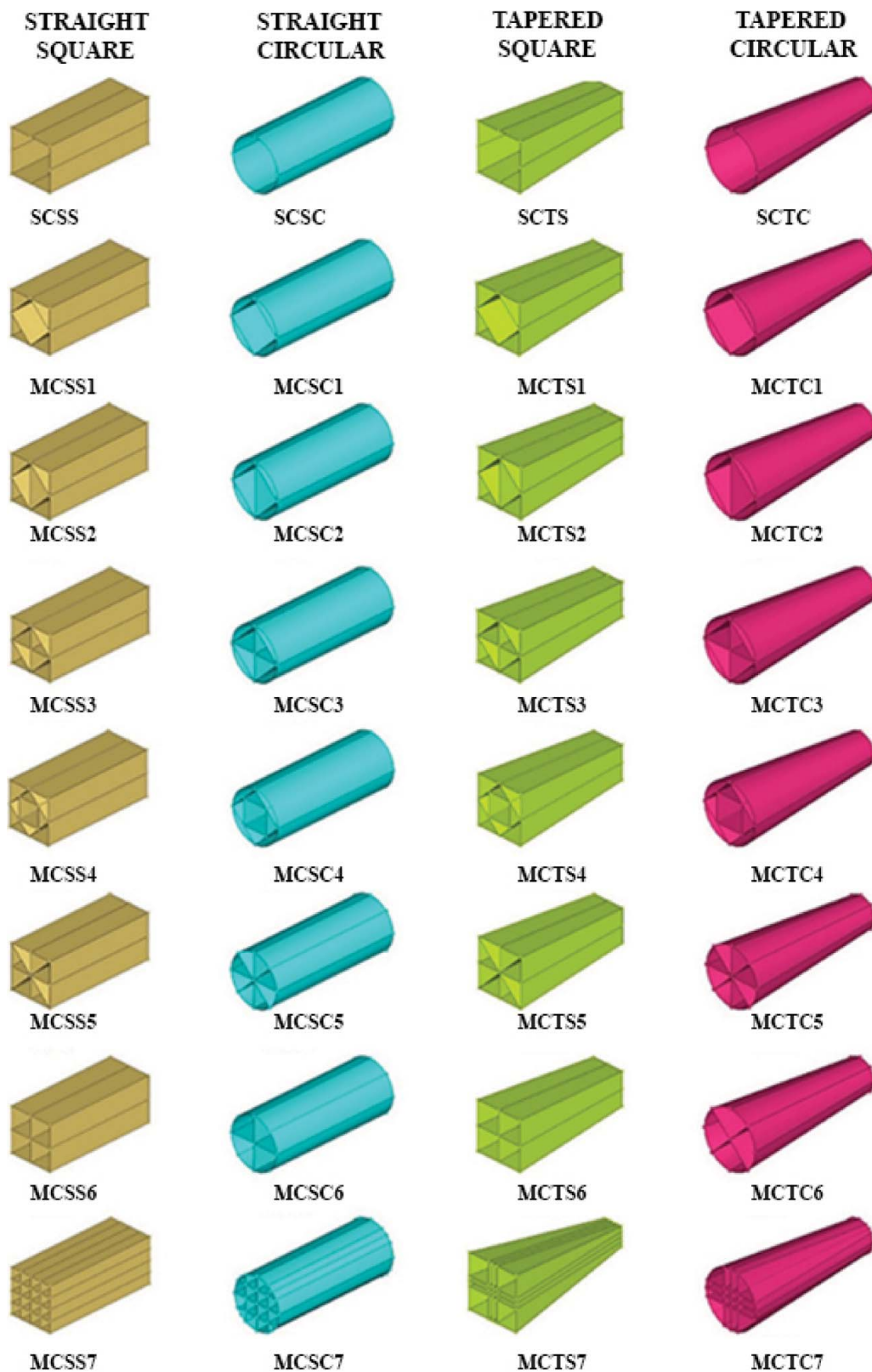
STRAIGHT SQUARE	STRAIGHT CIRCULAR	TAPERED SQUARE	TAPERED CIRCULAR
SCSS	SCSC	SCTS	SCTC
MCSS1	MCSC1	MCTS1	MCTC1
MCSS2	MCSC2	MCTS2	MCTC2
MCSS3	MCSC3	MCTS3	MCTC3
MCSS4	MCSC4	MCTS4	MCTC4
MCSS5	MCSC5	MCTS5	MCTC5
MCSS6	MCSC6	MCTS6	MCTC6
MCSS7	MCSC7	MCTS7	MCTC7

Figure 1. Different cell structures associated with four different types of multi-cell energy absorbers.

parameters were determined approximately by taking into consideration these literature values. The length of all types of energy absorbers is taken to be 180 mm. For square sections, the bottom edge length and for the circular sections, the bottom diameters are taken to be 72 mm. The selection of 180 mm for length and 72 mm for diameter is our personal preference, which is in the range of values used by many researchers in crash

studies. The design parameters of the energy absorbers are chosen as the wall thickness and the taper angle (i.e. the semi-epical angle). To explore the effect of the wall thickness, four different wall thickness values (1, 1.5, 2 and 2.5 mm) are used. To investigate the effect of the taper angle, four different taper angle values (0, 2.5°, 5° and 7.5°) are used. The design domains for thickness and taper angle are based on our earlier work [23,24].

In Figure 1, the abbreviation SC denotes the single-cell models, whereas MC denotes multi-cell models. For the single-cell models, the letters given after SC indicate the geometric properties of the tubes: SCSS model refers to the single-cell straight-square tube, SCSC model refers to the single-cell straight-circular tube, SCTS model refers to the single-cell tapered-square tube and SCTC model refers to the single-cell tapered-circular tube. Similarly, for the multi-cell models, the letters and the numbers given after MC indicate the geometric properties of the tubes as well as the cell structure used, respectively. For instance, MCTC3 stands for the multi-cell tapered-circular tube with cell structure number 3.

3. Finite element modelling

The commercially available explicit dynamic nonlinear FE analysis code LS-DYNA [25] is used to simulate the crush behaviour of the energy absorbers. The FE model is composed of three parts (see Figure 2). The first part is the bottom wall, which is a simplified model of the chassis of an automobile. The second part is the energy absorber that can have different types, shapes and dimensions. The third part is the rigid wall that has a velocity of 17.78 m/s (or 64 km/h) and a mass of 550 kg (40% of the mass of a standard vehicle) by following Euro NCAP regulations [26]. The initial kinetic energy of the rigid wall is approximately 87 kJ.

To study mesh convergence, different element sizes were used to discretise the circular and square tubes. The effect of mesh size effect on mean crush force, including total energy absorption and deformation distance are explored. Figure 3 and Table 1 present the
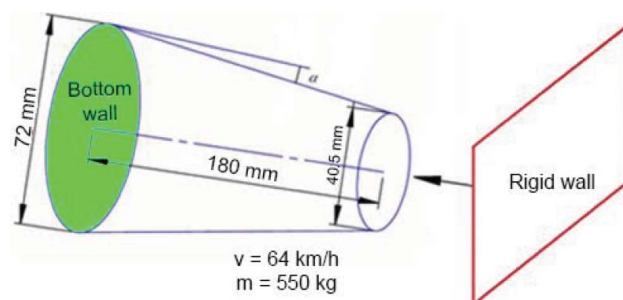
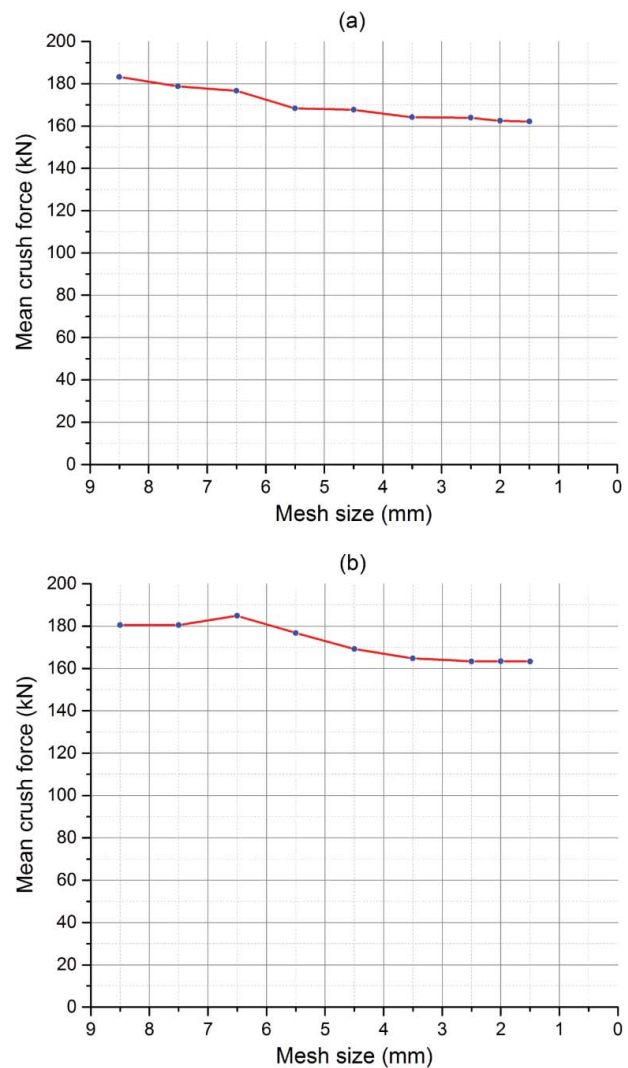

Figure 2. Rigid wall and the energy absorber.

Figure 3. Mean crush force of different element sizes used to discretise (a) SCSS and (b) SCSC tube.

mean crush force response from the FE models of square and circular tubes corresponding to element size 1.5–8.5 mm. It is found that the convergence is achieved at element size of 2.5 mm. In this study, the FE mesh is created by using the commercial mesh generation software HYPERMESH. Belytscko-Tsay shell element with five integration points is chosen.

LS-DYNA material library is used to define the material properties (MAT20 and MAT24). MAT20 is a rigid material and it is used to model the rigid wall at the end of the energy absorbers. MAT24 is selected for the material of the energy absorbers, and it is an elasto-plastic material in which the plastic regions can be included with true stress-effective plastic strain. strain curve. The energy absorbers are made of mild steel, and the Poisson's ratio, density and Young's modulus values are taken as 0.3, 7850 kg/m^3 and 210 GPa, respectively. Table 2 presents true effective stress-true effective plastic strain curve values for the selected steel. To incorporate

Table 1. Convergence of mean crush force versus mesh size for SCSS and SCSC models.

SCSS model		
Mesh size (mm)	Elements	Mean crush force (kN)
1.5	22,560	163.67
2	12,600	163.82
2.5	8352	164.03
3.5	4284	164.18
4.5	2560	167.69
5.5	1716	168.34
6.5	1232	176.7
7.5	960	178.78
8.5	672	183.17
SCSC model		
1.5	17,520	163.09
2	9900	163.15
2.5	6840	163.13
3.5	3264	163.18
4.5	2000	169.21
5.5	1386	176.83
6.5	952	184.88
7.5	720	180.55
8.5	546	180.53

Table 2. True effective stress-true effective plastic strain values for mild steel.

σ_t(MPa)	331	347	390	427	450	469	501	524	533	533
ε_p	0	0.018	0.0374	0.056	0.075	0.093	0.138	0.18	0.23	0.5

the strain rate effects, the following Cowper–Symonds relationship was used:

$$\dot{\varepsilon} = D\left(\frac{\sigma'_0}{\sigma_0} - 1\right)^q; \quad \sigma'_0 \geq \sigma_0 \tag{5}$$

where the constants D and q for strain rate effects are taken as 0.04 $(ms)^{-1}$ and 5, respectively, as in earlier studies [27,28]. The contact between the moving rigid wall and the absorber is 'Automatic single surface'. The static and dynamic friction coefficients for the absorber are taken as 0.3 and 0.2, respectively.

As an example to different types of energy absorbers, the geometric details of the tapered-circular energy
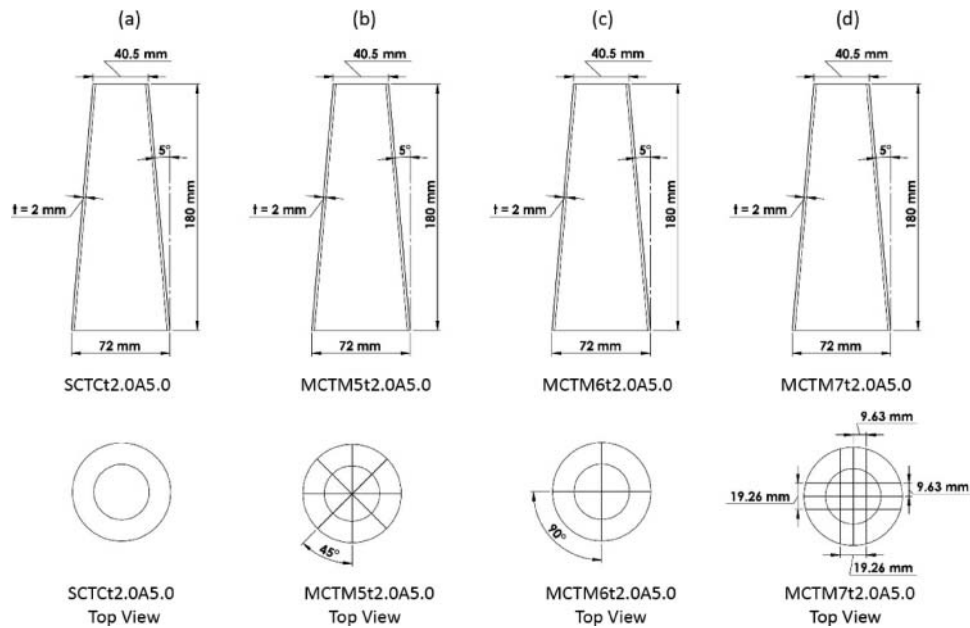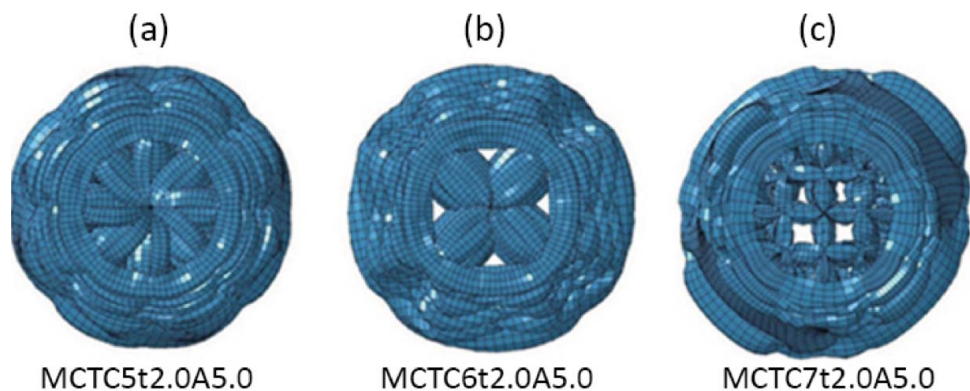

Figure 4. The geometric details of the tapered-circular energy absorbers: (a) SCTCt2.0A5.0; (b) MCTC5t2.0A5.0; (c) MCTC6t2.0A5.0; (d) MCTC7t2.0A5.0.

Figure 5. Simulation-based deformed shapes of the tapered-circular energy absorber with 2 mm thickness and 5⁰ taper angle: (a) MCTC5t2.0A5.0; (b) MCTC6t2.0A5.0; (c) MCTC7t2.0A5.0.

Table 3. The details of the geometries used in the validation study [13].

	Specimen 1	Specimen 2	Specimen 3	Specimen 4
Base dimensions (face × seam) (mm)	34.5 × 35.6	35.7 × 36.4	26.5 × 27.5	11.7 × 11.6
Top dimensions (face × seam) (mm)	50.0 × 51.9	58.5 × 59.1	55.8 × 57.2	56.8 × 56.5
Height (mm)	127	127	127	127
Wall thickness (mm)	0.97	1.47	1.6	1.52
Semi apical angle (°)	5°	7.5°	10°	14°
Number of shell elements	3300	3300	2000	4400
Drop mass (kg)	60	60	60	60
Impact velocity (m/s)	6.05	9.1	9.25	8.7

Table 4. Comparison of total energy absorption, initial peak force, specific energy absorption, number of lobe formation results for frusta with those from previously established solutions.

	Semi-apical angle, α (deg)	5	7.5	10	14
	Comparison of the total energy absorption				
Mamalis et al. [29] experimental	Total energy absorption (kJ)	0.896	1.792	1.716	1.738
Mamalis et al. [29] Numerical	Total energy absorption (kJ)	0.910	2.011	2.061	1.812
	Error (%)	1.5	12.2	**15.0**	4.2
Present study Numerical	Total energy absorption (kJ)	0.894	2.034	1.930	1.585
	Error (%)	0.3	**13.5**	11.1	8.8
	Comparison of the initial peak force				
Mamalis et al. [29] experimental	Initial peak force (kN)	36.50	63.37	50.43	29.3
Mamalis et al. [29] Numerical	Initial peak force (kN)	33.44	68.41	52.82	35.98
	Error (%)	8.3	7.9	4.7	**22.7**
Present study Numerical	Initial peak force (kN)	33.94	53.63	45.24	25.56
	Error (%)	8.3	**15.3**	10.0	12.7
	Comparison of the specific energy absorption				
Mamalis et al. [29] experimental	Specific energy absorption (kJ/kg)	5.517	6.642	6.672	8.675
Mamalis et al. [29] Numerical	Specific energy absorption (kJ/kg)	5.600	7.455	8.011	9.043
	Error (%)	1.5	12.2	**15.0**	4.2
Present study Numerical	Specific energy absorption (kJ/kg)	5.503	7.540	7.503	7.909
	Error (%)	0.3	**13.5**	11.1	8.8
	Comparison of the number of lobe formation				
Mamalis et al. [29] experimental	Number of lobe formation	4	4	4	5
Mamalis et al. [29] Numerical	Number of lobe formation	4	4	5	4
	Error (%)	0	0	**20**	**20**
Present study Numerical	Number of lobe formation	4	4	5	4
	Error (%)	0	0	**20**	**20**

Note: All values are computed at a cut-off crush distance, $\delta_c = 70$ mm. The bold fonts indicate the maximum error corresponding to the metric of comparison.
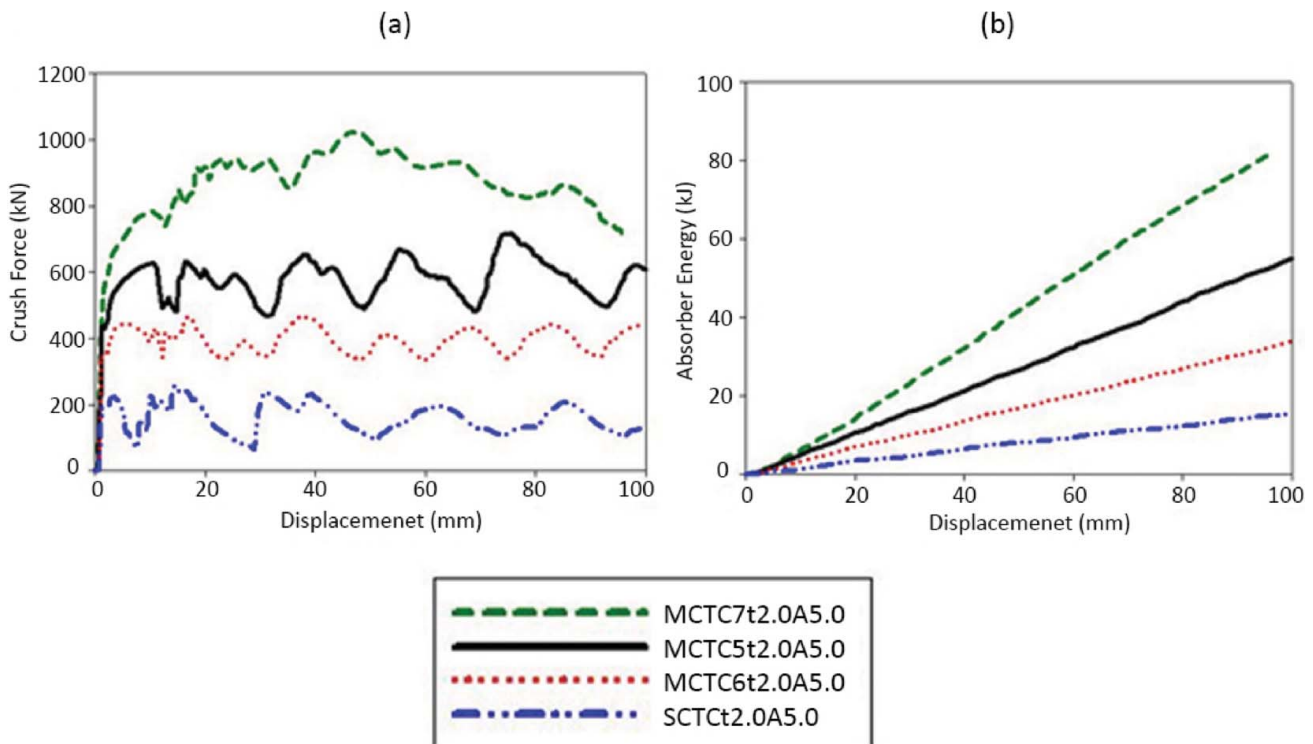

Figure 6. Comparison between the crush force-displacement (a), and the absorbed energy (b) for selected tapered-circular absorber geometries with the corresponding baseline model.

absorbers are shown in Figure 4. Using these geometric details, FE models of these absorbers are generated and crash simulations are performed by using LS-DYNA. The deformed shapes of the tapered-circular energy absorber models with 2 mm thickness and 5° taper angle are shown in Figure 5. Comparison of the crush force-displacement and the absorbed energy for some selected tapered-circular absorber geometries with the corresponding baseline model (SCTC) are presented in Figure 6. It is seen that the multi-cell designs have better crush force efficiencies and better energy absorption capabilities than the single-cell (baseline) design. It is observed that the multi-cell design MCTC7 displays the best performance amongst the multi-cell designs considered for this illustration.

4. Validation of the FEA model

The FEA model of the tapered-square energy absorber model (i.e. SCTS) was validated by using the results presented by Mamalis et al. [29]. We regenerated Mamalis' models following the presented modelling approach, and we ran the simulation and compared the results. The geometry considered in Mamalis et al. [29] was a frusta of 127-mm length and semi-apical angles of 5°, 7.5°, 10° and 14°. The details of the geometries used in the validation study are given in Table 3. The comparison of the FEA results (total energy absorption, initial peak force, SEA, number of lobe formation) obtained in this study and the results presented in [29] are given in Table 4. Note that all the SEA and CFE calculations are
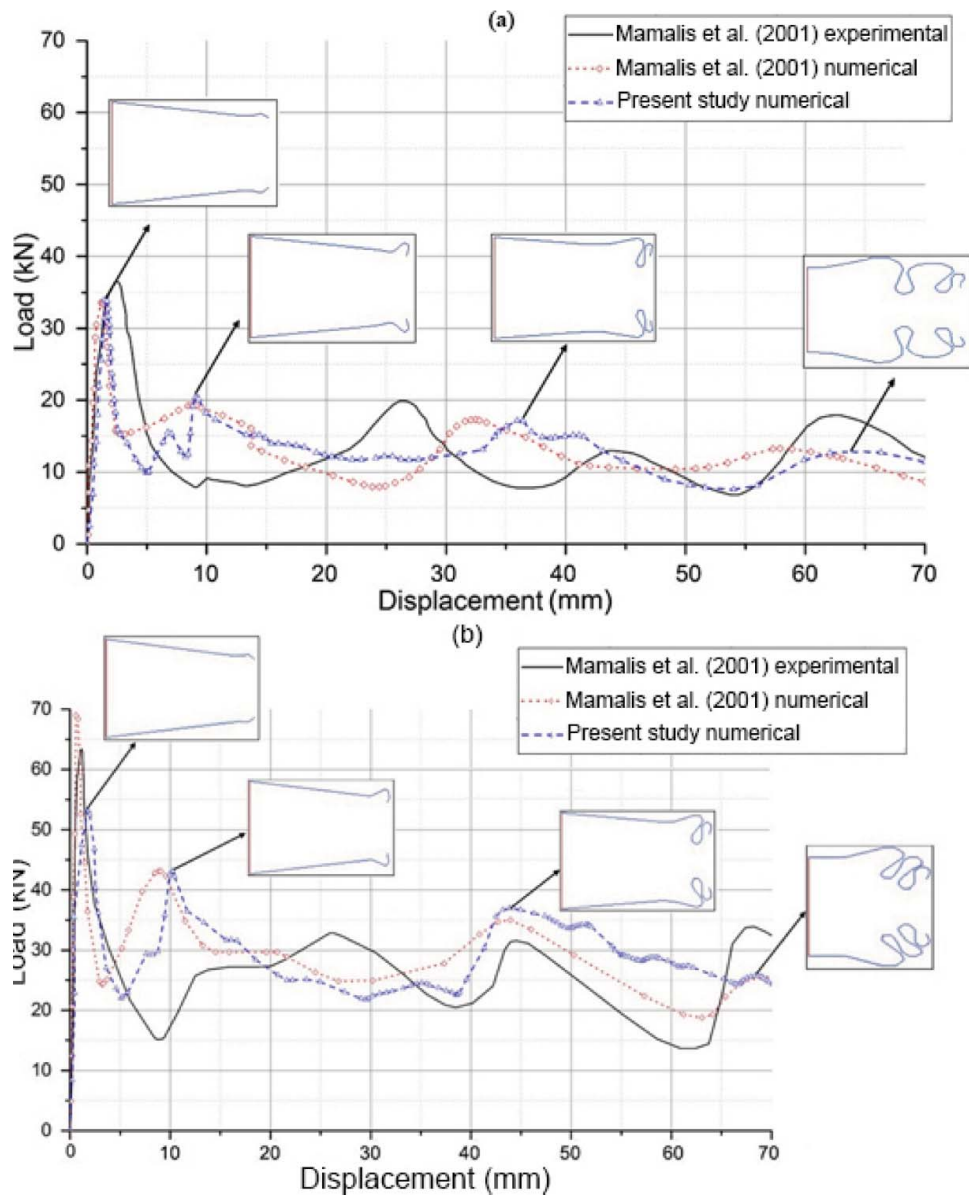

Figure 7. Load-displacement curves for tapered tube: Specimen 1 (a); Specimen 2 (b) (see Table 3).

based on cut-off distance of crush of $\delta_c = 70$ mm. Table 4 shows that the maximum errors in prediction of the crush responses using the FEA model of this study are all smaller than those of the FEA model of Mamalis et al. [29]. For instance, the maximum error in total energy absorption prediction using the FEA model of Mamalis et al. [29] is 15.0%, whereas the corresponding maximum error for the FEA model of this study is 13.5%. The maximum error in initial peak force prediction using the FEA model of Mamalis et al. [29] is 22.7%, whereas the corresponding maximum error for the FEA model of this study is only 15.3%. It can also be seen from the crushing force histories in Figures 7 and 8 that for load-displacement curves, the simulation results were generally in good agreement with experimental results.

5. Results and discussion

In this section, first, the crush performances of four different types of cross-sectional geometry are evaluated and compared to each other. Then, the effects of wall thickness and the taper angle are explored.

5.1. Effect of the multi-cell structure

The crush performances of different multi-cell structures are evaluated by using the metrics defined in Section 2. The wall thickness is set to 1.5 mm, and the taper angle is set to 5° (for tapered tubes). The CFE and SEA results for different multi-cell design configurations are presented in Tables 5–8. The abbreviated symbols given in Tables 5–8 are used to identify different types of models
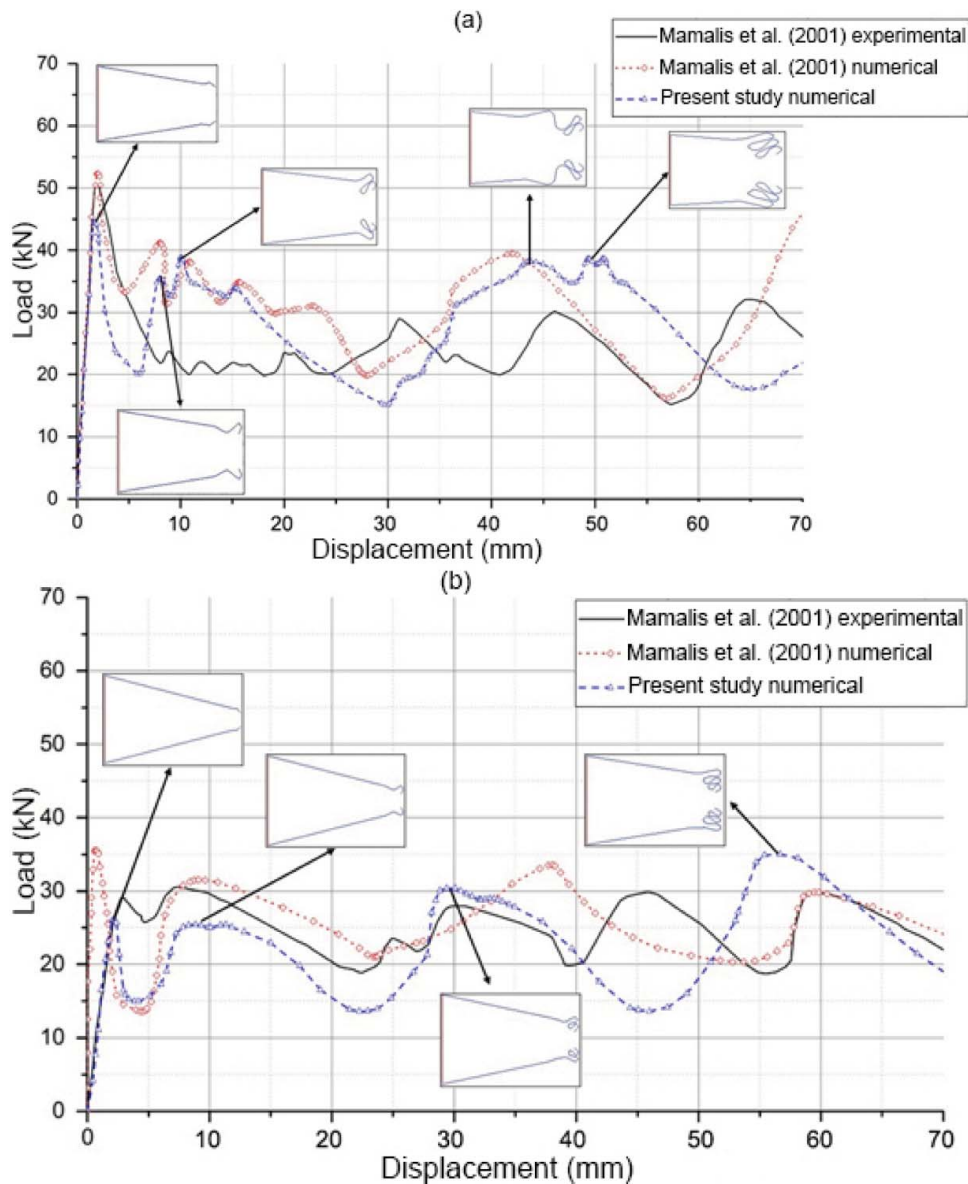

Figure 8. Load-displacement curves for tapered tube: Specimen 3 (a); Specimen 4 (b) (see Table 3).

Table 5. Crush performances of straight-square geometries.

Model name	Energy (kJ)	Peak crush force (kN)	Mean crush force (kN)	CFE	% Difference in CFE	SEA (kJ/kg)	% Difference in SEA
SCSSt1.5A0	9.93	314.0	99.4	0.316	0	16.74	0
MCSS1t1.5A0	24.35	540.4	243.6	0.451	43	24.04	44
MCSS2t1.5A0	28.62	618.6	286.3	0.463	47	24.64	47
MCSS3t1.5A0	36.15	698.9	315.5	0.517	64	27.60	65
MCSS4t1.5A0	38.71	696.9	387.2	0.555	76	29.56	77
MCSS5t1.5A0	35.14	704.9	351.4	0.499	58	26.83	60
MCSS6t1.5A0	23.99	474.0	240.0	0.506	60	26.95	61
MCSS7t1.5A0	67.82	928.6	678.3	0.730	131	45.72	173

Table 6. Crush performances of straight-circular geometries.

Model name	Energy (kJ)	Peak crush force (kN)	Mean crush force (kN)	CFE	% Difference in CFE	SEA (kJ/kg)	% Difference in SEA
SCSCt1.5A0	10.51	242.9	105.1	0.433	0	22.56	0
MCSC1t1.5A0	25.20	466.0	252.1	0.541	25	28.46	26
MCSC2t1.5A0	27.92	545.8	279.3	0.512	18	27.00	20
MCSC3t1.5A0	34.78	626.1	347.8	0.555	28	29.42	30
MCSC4t1.5A0	38.32	628.6	383.2	0.610	41	32.41	44
MCSC5t1.5A0	36.14	594.4	361.4	0.608	40	34.11	51
MCSC6t1.5A0	23.16	409.1	231.9	0.566	31	30.39	35
MCSC7t1.5A0	59.27	789.8	592.8	0.750	73	46.43	106

(see Figure 1 for the description of different multi-cell geometries). In model descriptions, 't***' is used to define the wall thickness and 'A***' is used to define the taper angle. For instance, MCSS1t1.5A0 is the model with multi-cell straight-square geometry that has 1.5 mm wall thickness and 0 taper angle, whereas MCTC7t1.5A5.0 is the model with multi-cell tapered-circular geometry that has 1.5 mm wall thickness and 5.0° taper angle.

Tables 5 and 6 present the results for the straight-square and straight-circular geometries. Table 5 shows that multi-cell straight-square designs have 43%–131% larger CFE, and 44%–173% larger SEA compared to single-cell straight-square designs. Table 6 shows that multi-cell straight-circular designs have 18%–73% larger CFE, and 20%–106% larger SEA compared to single-cell straight-circular designs.

The results for the tapered-square and tapered-circular geometries are presented in Tables 7 and 8. Table 7 depicts that multi-cell tapered-square designs have 47%–109% larger CFE, and 53%–191% larger SEA compared to single-cell tapered-square designs. Table 8 shows that multi-cell tapered-circular designs have 12%–43% larger CFE, and 26%–153% larger SEA compared to single-cell tapered-circular designs.

From Tables 5–8 and Figures 9 and 10, it can be inferred that the multi-cell design having the best CFE performance (MCTC7t1.5A5.0 design) has a CFE value of 0.836. This value is 165% larger than the single-cell design having the worst performance (SCSS1.5A0

Table 7. Crush performances of tapered-square geometries.

Model name	Energy (kJ)	Peak crush force (kN)	Mean crush force (kN)	CFE	% Difference in CFE	SEA (kJ/kg)	% Difference in SEA
SCTSt1.5A5.0	9.13	234.8	91.3	0.389	0	18.26	0
MCTS2t1.5A5.0	27.37	479.8	273.6	0.570	47	27.97	53
MCTS3t1.5A5.0	35.53	544.2	355.1	0.653	68	32.20	76
MCTS4t1.5A5.0	39.92	547.7	399.9	0.729	87	36.26	99
MCTS5t1.5A5.0	35.28	583.9	352.8	0.604	55	31.77	74
MCTS6t1.5A5.0	23.57	373.6	235.8	0.631	62	31.45	72
MCTS7t1.5A5.0	66.34	816.1	663.4	0.813	109	53.14	191

Table 8. Crush performances of tapered-circular geometries.

| Model name	Energy (kJ)	Peak crush force (kN)	Mean crush force (kN)	CFE	% Difference in CFE	SEA (kJ/kg)	% Difference in SEA
SCTCt1.5A5.0	9.36	159.8	93.7	0.586	0	25.84	0
MCTC1t1.5A5.0	24.82	362.5	248.3	0.684	17	36.07	40
MCTC2t1.5A5.0	26.15	371.3	261.5	0.704	20	32.55	26
MCTC3t1.5A5.0	34.36	430.6	343.6	0.798	36	37.41	45
MCTC4t1.5A5.0	36.34	556.0	363.5	0.654	12	39.57	53
MCTC5t1.5A5.0	34.31	445.4	343.1	0.770	31	41.71	61
MCTC6t1.5A5.0	21.18	285.8	211.8	0.741	26	35.74	38
MCTC7t1.5A5.0	57.58	688.9	575.9	0.836	43	56.37	153
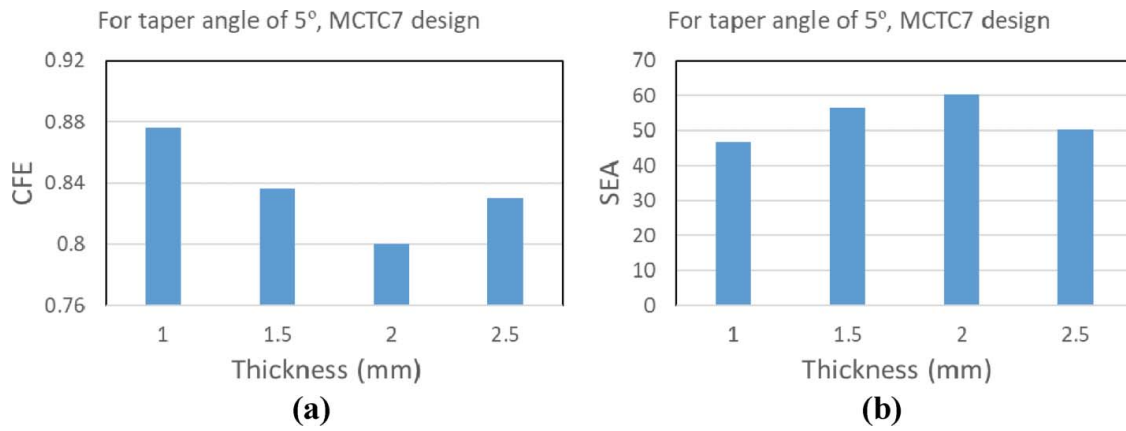
Figure 9. Effect of wall thickness on (a) CFE and (b) SEA for MCTC7 design when taper angle is 5°.

design) with a CFE value of 0.316. Similarly, the multi-cell design having the best SEA performance (MCTC7t1.5A5.0 design) has a SEA value of 56.37 kJ/kg. This value is 237% larger than the single-cell design having the worst performance (SCSS1.5A0 design) with a SEA value of 16.74 kJ/kg. Note that the MCTC7t1.5A5.0 design has the best performance in terms of both CFE and SEA.

5.2. Effect of the wall thickness

In the previous section, it is found that the multi-cell tapered-circular (MCTC) energy absorber models display the best crush performance; therefore this specific model is used for further investigation. To explore the effect of the wall thickness, four different wall thickness values (1, 1.5, 2 and 2.5 mm) are used, whereas the taper angle is set to 5°. The results of the FE simulations are given in Table 9 and Figure 11. It is found for any given cell structure that as the wall thickness increases from 1 to 2.5 mm, SEA increases. The relationship between the wall thickness and CFE is found to be rather complex. For instance, for MCTC1 cell structure, CFE increases from 0.654 to 0.704 when the thickness increases from 1 to 2 mm, and almost stays constant around 0.70 for further increase of thickness from 2 to 2.5 mm. On the

Table 9. The effect of wall thickness on the crush performance of multi-cell tapered-circular energy absorber models.

Model name	Energy (kJ)	Peak crush force (kN)	Mean crush force (kN)	CFE	SEA (kJ/kg)
MCTC1t1.0A5.0	12.86	196.7	128.6	0.654	28.01
MCTC2t1.0A5.0	13.27	228.3	132.7	0.581	24.77
MCTC3t1.0A5.0	16.78	265.1	167.8	0.633	27.41
MCTC4t1.0A5.0	19.94	299.2	199.4	0.666	32.56
MCTC5t1.0A5.0	17.77	273.4	177.7	0.650	32.41
MCTC6t1.0A5.0	11.15	179.1	111.5	0.623	28.22
MCTC7t1.0A5.0	31.98	364.9	319.8	**0.876**	46.96
MCTC1t1.5A5.0	24.83	362.5	248.3	0.685	36.07
MCTC2t1.5A5.0	26.15	371.3	261.5	0.704	32.55
MCTC3t1.5A5.0	34.36	430.6	343.6	0.798	37.42
MCTC4t1.5A5.0	36.35	556.0	363.5	0.654	39.57
MCTC5t1.5A5.0	34.31	445.4	343.1	0.770	41.72
MCTC6t1.5A5.0	21.18	285.8	211.8	0.741	35.75
MCTC7t1.5A5.0	57.59	688.9	575.9	0.836	56.37
MCTC1t2.0A5.0	39.44	559.9	394.4	0.704	42.97
MCTC2t2.0A5.0	43.02	523.9	430.2	0.821	40.16
MCTC3t2.0A5.0	56.03	719.3	560.3	0.779	45.76
MCTC4t2.0A5.0	56.73	833.1	567.3	0.681	46.32
MCTC5t2.0A5.0	55.20	720.9	552.0	0.766	50.33
MCTC6t2.0A5.0	34.12	421.9	341.2	0.809	43.19
MCTC7t2.0A5.0	82.08	1026.6	854.1	0.800	**60.27**
MCTC1t2.5A5.0	54.51	780.1	545.1	0.700	47.51
MCTC2t2.5A5.0	60.62	784.6	606.2	0.773	45.28
MCTC3t2.5A5.0	77.97	997.2	780.0	0.782	50.96
MCTC4t2.5A5.0	78.40	1097.4	784.0	0.714	51.60
MCTC5t2.5A5.0	77.09	921.3	770.9	0.837	56.23
MCTC6t2.5A5.0	48.99	611.5	489.9	0.801	49.61
MCTC7t2.5A5.0	85.31	1364.8	1128.2	0.830	50.11*

Note: The SEA value corresponding to this design is not countable as the whole kinetic energy is converted to deformation energy before 100 mm collapse of the corresponding design. The numbers with bold fonts show the maximum value observed in the corresponding column.
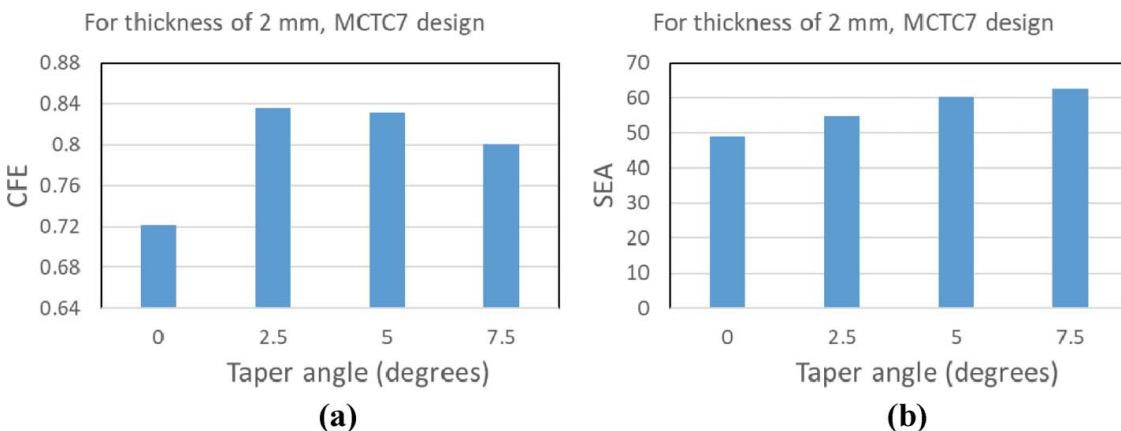

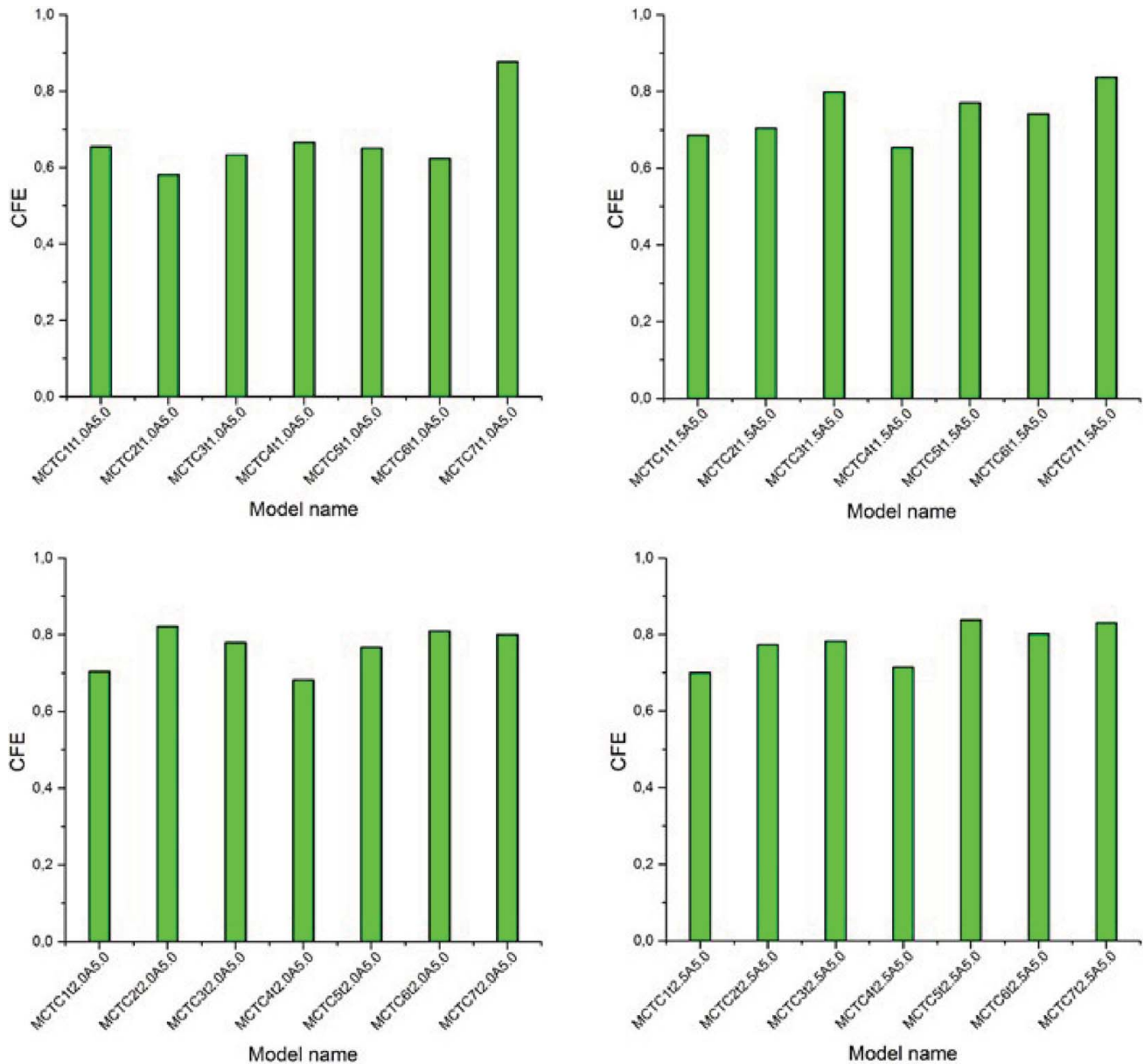Figure 10. Effect of taper angle on (a) CFE and (b) SEA for MCTC7 design when wall thickness is 2 mm.

Figure 11. The graphical depiction of the effect of wall thickness on the crash performance of multi-cell tapered-530 circular energy absorber models.

other hand, for MCTC2 cell structure, CFE increases from 0.581 to 0.821 when the thickness increases from 1 to 2 mm, but reduces to 0.773 for further increase of thickness from 2 to 2.5 mm. Table 9 shows also that the cell structure that has the best crush performance is found to be MCTC7 cell structure. MCTC7 cell structure with 1 mm wall thickness has the maximum CFE (CFE = 0.876), whereas MCTC7 cell structure with 2 mm wall thickness has the maximum SEA (SEA = 60.27 kJ/kg). It should also be noted here that the SEA value corresponding to 2.5 mm wall thickness does not reflect the true potential of energy absorption of this design as the whole kinetic energy

is converted to deformation energy before 100 mm collapse of the corresponding design.

Table 9 also shows that by varying the thickness, the CFE and SEA performances of the multi-cell designs can be further increased. In terms of CFE, it is seen that maximum CFE value is attained by MCTC71.0A5.0 design with CFE = 0.876, which is 5% greater than the CFE of MCTC7t1.5A5.0 design (CFE = 0.836) that was found as the best design in Section 5.1. In terms of SEA, it is seen that the maximum SEA value is attained by MCTC7t2.0A5.0 design with SEA = 60.27 kJ/kg, which is 7% greater than the SEA of MCTC7t1.5A5.0 design (SEA = 56.37 kJ/kg).
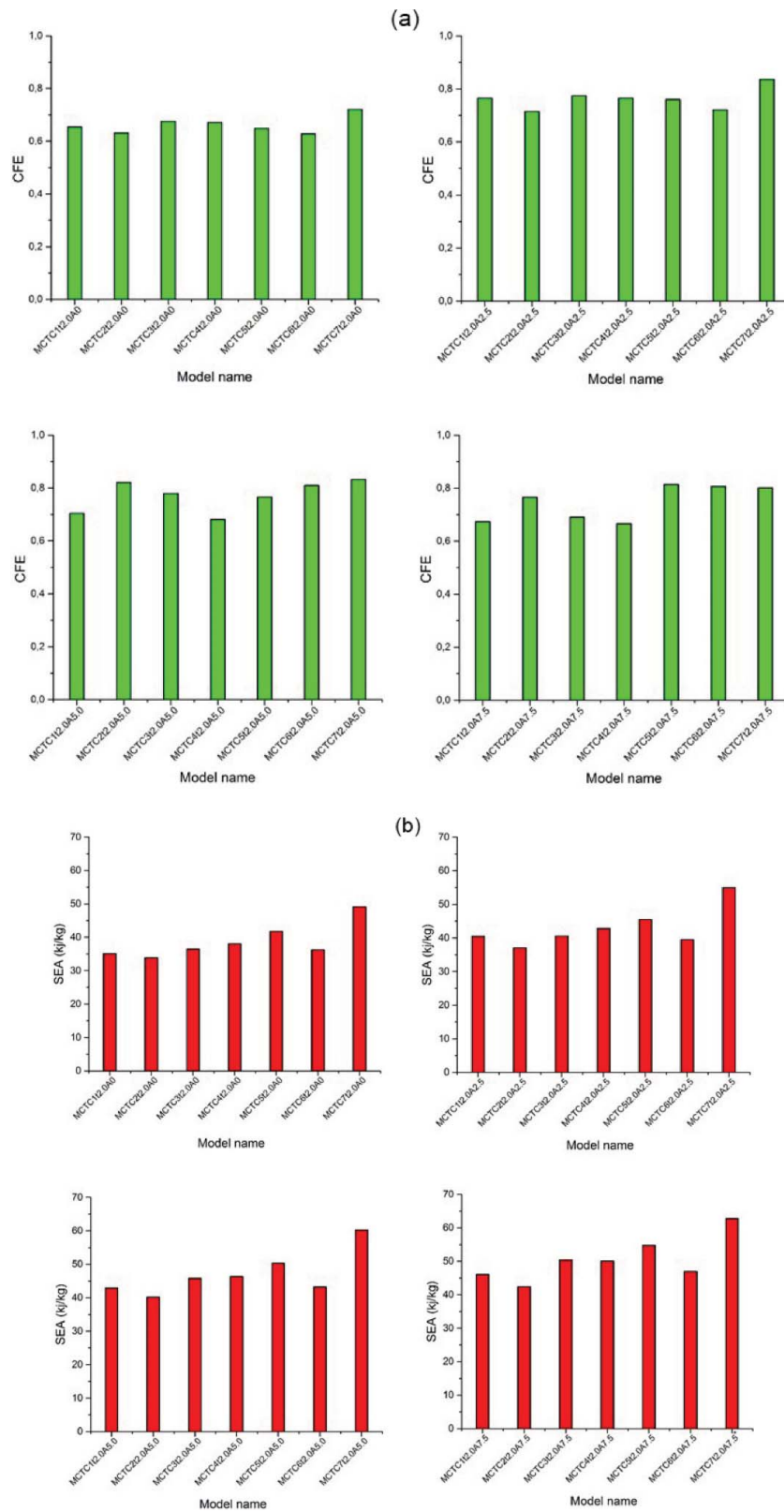
Figure 12. The graphical depiction of the effect of taper angle on the crash performance of multi-cell tapered-530 circular energy absorber models.

5.3. Effect of taper angle

To explore the effect of taper angle, four different taper angle values (0, 2.5°, 5° and 7.5°) are used, whereas the wall thickness is set to 2 mm. Table 10 presents the results of FE simulations. Table 10 and Figure 12 show for any given cell structure that as the taper angle increases from 0 to 7.5°, SEA increases. Similar to the discussion in Table 9, the relationship between the taper angle and CFE is rather complex. It is observed that at first the CFE increases as the taper angle is increased from 0 to a specific value, and then the CFE reduces for further increase of the taper angle. For instance, for MCTC1 cell structure, CFE increases from 0.654 to 0.765 when the taper angle increases from 0 to 2.5°, but reduces to 0.704 and then to 0.673 when the taper angle further increases to 5° and then to 7.5°. On the other hand, for MCTC2 cell structure, CFE increases from 0.63 to 0.82 when the taper angle increases from 0 to 5°, but reduces to 0.76 for further increase of taper angle from 5° to 7.5°.

Table 10 also shows that by varying the taper angle, the SEA performance of the best design in Table 9 (SEA = 60.27 kJ/kg) can further be increased to SEA = 62.80 kJ/kg, which corresponds to about 4% improvement. On

Table 10. The effect of taper angle on the crush performance of multi-cell tapered-circular energy absorber models.

Model name	Energy (kJ)	Peak crush force (kN)	Mean crush force (kN)	CFE	SEA (kJ/kg)
MCTC1t2.0A0	41.42	633.1	414.3	0.654	35.07
MCTC2t2.0A0	46.74	740.0	467.4	0.632	33.90
MCTC3t2.0A0	57.47	851.1	574.7	0.675	36.45
MCTC4t2.0A0	59.88	892.7	598.9	0.671	37.98
MCTC5t2.0A0	58.98	909.4	589.9	0.649	41.75
MCTC6t2.0A0	36.88	587.4	368.8	0.628	36.26
MCTC7t2.0A0	83.68	1160.5	928.1	0.721	49.15
MCTC1t2.0A2.5	42.46	555.3	424.7	0.765	40.49
MCTC2t2.0A2.5	45.33	634.2	453.4	0.715	37.03
MCTC3t2.0A2.5	56.74	733.1	567.5	0.774	40.54
MCTC4t2.0A2.5	59.88	782.3	598.9	0.765	42.78
MCTC5t2.0A2.5	56.97	749.4	569.8	0.76	45.44
MCTC6t2.0A2.5	35.67	495.0	356.8	0.721	39.51
MCTC7t2.0A2.5	84.33	1100.1	919.5	**0.836**	54.99
MCTC1t2.0A5.0	39.43	559.9	394.4	0.704	42.96
MCTC2t2.0A5.0	43.02	523.9	430.2	0.821	40.16
MCTC3t2.0A5.0	56.03	719.3	560.3	0.779	45.75
MCTC4t2.0A5.0	56.73	833.1	567.3	0.681	46.31
MCTC5t2.0A5.0	55.19	720.9	552.0	0.766	50.33
MCTC6t2.0A5.0	34.11	421.9	341.2	0.809	43.18
MCTC7t2.0A5.0	82.08	1026.6	854.1	0.832	60.27
MCTC1t2.0A7.5	36.20	537.8	362.0	0.673	46.05
MCTC2t2.0A7.5	38.85	507.1	388.5	0.766	42.36
MCTC3t2.0A7.5	52.81	765.2	528.2	0.690	50.40
MCTC4t2.0A7.5	52.44	787.5	524.5	0.666	50.02
MCTC5t2.0A7.5	51.38	632.4	513.9	0.813	54.79
MCTC6t2.0A7.5	31.76	394.1	317.6	0.806	46.97
MCTC7t2.0A7.5	74.19	926.0	742.0	0.801	**62.80**

Note: The numbers with bold fonts show the maximum value observed in the corresponding column.

(a)

t=0 ms   t=1.5 ms   t=3.0 ms   t=4.5 ms   t=6.0 ms   t=7.5 ms   t=9.0 ms

(b)

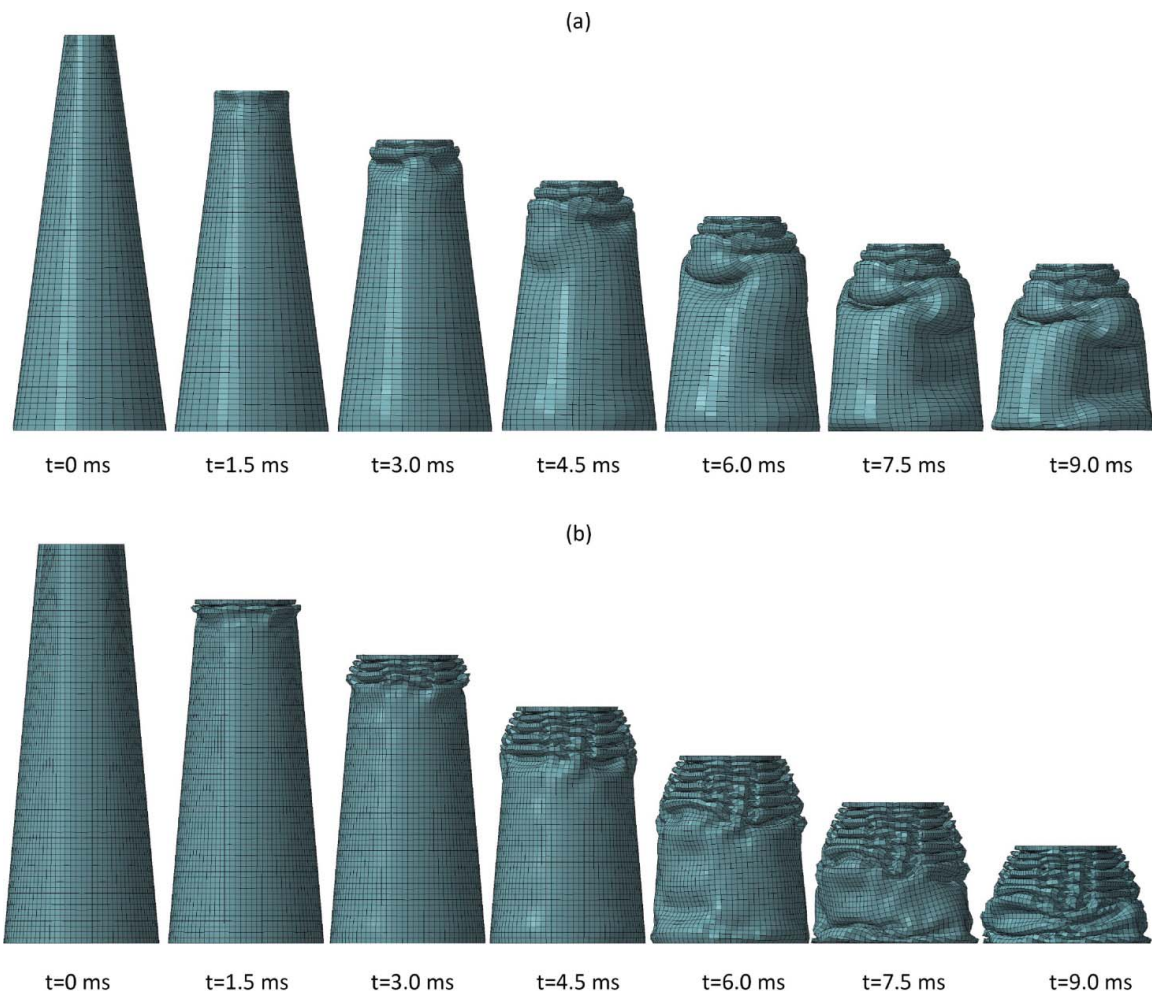t=0 ms   t=1.5 ms   t=3.0 ms   t=4.5 ms   t=6.0 ms   t=7.5 ms   t=9.0 ms

Figure 13. Progressive collapse of model (a) MCTC7t2.0A7.5 type and (b) MCTC7t1.0A5.0 type of multi-cell structures.
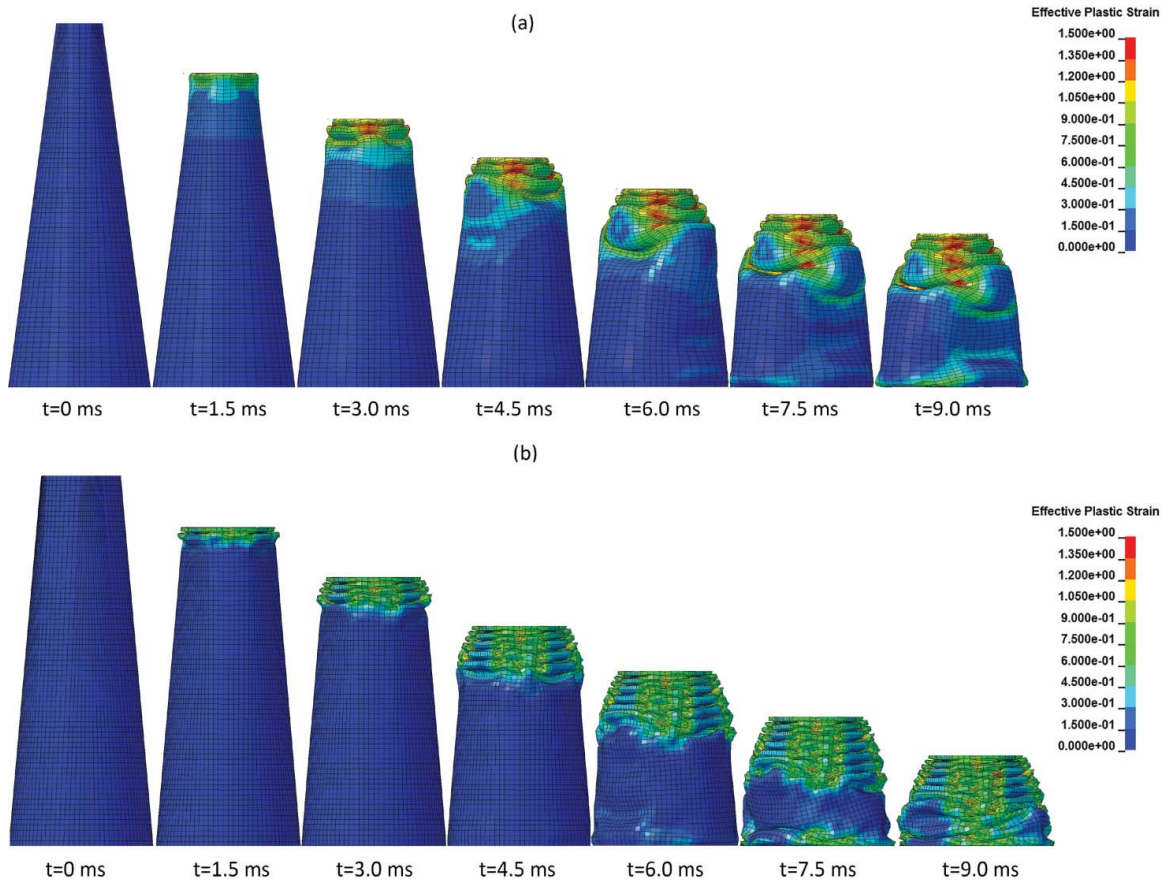
Figure 14. Plastic strains of the model (a) MCTC7t2.0A7.5 type and (b) MCTC7t1.0A5.0 type of multi-cell structures during collapse.

the other hand, there is no further increase on the CFE value of the best design in Table 9 as the taper angle is varied.

Finally, the progressive collapse and plastic strain distribution during collapse of the best design in terms of CFE (MCTC7t1.0A5.0 design) as well as the best design
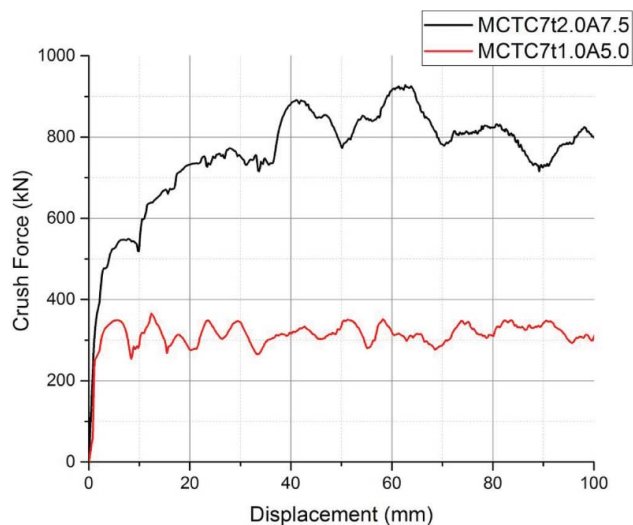
in terms of SEA (MCTC7t2.0A7.5 design) are shown in Figures 13 and 14, respectively. The best CFE design has better collapse behavior but it has smaller energy absorption due to its smaller thickness compared to the best SEA design. The force-displacement curves for the best CFE and SEA designs are shown in Figure 15. The best CFE design has a peak crush force of 364.9 kN, and mean crush force of 319.8 kN as compared to the best SEA design that has a peak crush force of 926.0 kN, and mean crush force of 742.0 kN.

Figure 15. Force-displacement curves for MCTC7t2.0A7.5 type and MCTC7t1.0A5.0 type multi-cell structures.

6. Conclusions

In this paper, crush performances of multi-cell columns with different geometric properties and different cell structures were assessed by using explicit dynamic non-linear FE analysis code LS-DYNA. The crashworthiness assessment was based on two different metrics: the CFE and the SEA. From the results obtained, the following conclusions were drawn:

- For a given type of energy absorber model (straight-square, straight-circular, tapered-square or tapered-circular models), all multi-cell models

had larger CFE and SEA values than the single-cell models. As an example, for straight-square models, the multi-cell geometries with best performance have 2.3 times larger CFE values and 2.7 times larger SEA values compared to the single-cell model. Similarly, for straight-circular models, the multi-cell geometries with best performance have 1.7 times larger CFE values and 2.1 times larger SEA values compared to the single-cell model.

- For a wall thickness of 1.5 mm and a taper angle of 5° configurations (the baseline configuration used in this study), the tapered-circular models displayed the best crush performance. The multi-cell design having the best CFE performance has a CFE value 2.7 times larger than the single-cell design having the worst performance. Similarly, the multi-cell design having the best SEA performance has a SEA value 3.4 times larger than the single-cell design having the worst performance. It is also found that the MCTC7 type design has the maximum crush performance in terms of both CFE and SEA values.
- For any given cell structure, as the wall thickness and taper angle increased within the range of values considered only in this study, SEA also increased accordingly.
- The relationship between the wall thickness and CFE was rather complex. For some cell structures, CFE increased up to a specific value and then stayed constant. For other cell structures, CFE first increased up to a specific value and then reduced.
- Similarly, the relationship between the taper angle and CFE was also complex. It was observed that the CFE increased as the taper angle was increased up to a specific value, and then the CFE reduced for further increase of the taper angle.

For real-life applications, the users need to consider high cost involved in manufacturing of the complex structure of multi-cell designs. The users need to consider the cost-performance trade-offs and make their decision on the use of multi-cell designs over single-cell designs accordingly. It has been shown in the literature that the use of metallic foams in tubes can significantly increase the energy absorption capability. In a future research, the effect of using a cellular foam structure on the crush performance of multi-cell energy absorbers could be investigated. In addition, optimisation of multi-cell energy absorbers for maximum crush performance can be performed in a follow-up study.

Acknowledgement

Disclosure statement

No potential conflict of interest was reported by the authors.

Funding

ORCID

Mehmet Ali Güler http://orcid.org/0000-0003-4814-5834

References

[1] H Eifert. C Yu, J Banhart, et al. Weight savings by aluminum metal foams: production, properties and applications in automotive. 1999. p. 1–8. (SAE Technical Papers).

[2] , Y Nakazawa, K Tamura, M Yoshida, et al., F Development of crash-box for passenger car with high capability for energy absorption. Proceedings of the 8th International Conference on Computational Plasticity, COMPLAS VIII, CIMNE; Part 1 ed.; 2005. p. 577–580, Barcelona, Spain., E Onate, DRJ Owen

[3] H-S Kim, T Wierzbicki. Effect of the cross-sectional shape on crash behavior of a three dimensional space frame. Int J Veh Des. 25:2001;283–304.

[4] H-S Kim. New extruded multi-cell aluminum profile for maximum crash energy absorption and weight efficiency. Thin Wall Struct. 40:2002;311–327.

[5] A Baroutajia, M Sajjiab, A-G Olabic. On the crashworthiness performance of thin-walled energy absorbers: recent advances and future developments. Thin Wall Struct. 118:2017;137–163.

[6] A Alavi Nia, M Parsapour. Comparative analysis of energy absorption capacity of simple and multi-cell thin-walled tubes with triangular, square, hexagonal and octagonal sections. Thin Wall Struct. 74:2014;155–165.

[7] A Jusuf, T Dirgantara, L Gunawan, et al. Crashworthiness analysis of multi-cell prismatic structures. Int J Impact Eng. 78:2015;34–50.

[8] SJ Hou, Q Li, SY Long, et al. Multiobjective optimization of multi-cell sections for the crashworthiness design. Int J Impact Eng. 35:2008;1355–1367.

[9] A Najafi, M Rais-Rohani. Mechanics of axial plastic collapse in multi-cell, multi-corner crush tubes. Thin Wall Struct. 49:2011;1–12.

[10] A Alavi Nia, M Parsapour. An investigation on the energy absorption characteristics of multi-cell square tubes. Thin Wall Struct. 68:2013;26–34.

[11] Z Tang, S Liu, Z Zhang. Analysis of energy absorption characteristics of cylindrical multi-cell columns. Thin Wall Struct. 62:2013;75–84.

[12] X Zhang, H Zhang. Energy absorption of multi-cell stub columns under axial compression. Thin Wall Struct. 68:2013;156–163.

[13] S Reid, T Reddy. Static and dynamic crushing of tapered sheet metal tubes of rectangular cross-section. Int J Mech Sci. 28:1986;623–637.

[14] C Qi, S Yang, F Dong. Crushing analysis and multi-objective crashworthiness optimization of tapered square tubes under oblique impact loading. Thin Wall Struct. 59:2012;103–119.

[15] A Mahmoodi, MH Shojaeefard, H Saeidi Googarchin. Theoretical development and numerical investigation on energy absorption behavior of tapered multi-cell tubes. Thin Wall Struct. 102:2016;98–110.

[16] X Zou, G Gao, H Dong, et al. Crashworthiness analysis and structural optimisation of multi-cell square tubes under axial and oblique loads. Int J Crashworthiness. 22:2017;129–147.

[17] Y-C Liu, ML Dag. Concept modeling of tapered thin-walled tubes. J Zhejiang Univ-Sci A. 10:2009;44–53.

[18] Y Liu. Design optimisation of tapered thin-walled square tubes. Int J Crashworthiness. 13:2008;543–550.

[19] Y Liu. Crashworthiness response and design of tapered thin-walled square beams. 2010 Research Bulletin of the Australian Institute of High Energetic Materials. 2010. p. 49–57.Australian Institute of High Energetic Materials, Australia.

[20] S Pirmohammad, SE Marzdashti. Crushing behavior of new designed multi-cell members subjected to axial and oblique quasi-static loads. Thin Wall Struct. 108:2016;291–304.

[21] J Fang, G Sun, N Qiu, et al. On design optimization for structural crashworthiness and its state of the art. Struct Multidiscip Optim. 55:2017;1091–1119.

[22] SY Jin, W Altenhof. Comparison of the load/displacement and energy absorption performance of round and square AA6061-T6 extrusions under a cutting deformation mode. Int J Crashworthiness. 12:2007;265–278.

[23] MA Guler, ME Cerit, B Bayram, et al. The effect of geometrical parameters on the energy absorption characteristics of thin-walled structures under axial impact loading. Int J Crashworthiness. 15:2010;377–390.

[24] E Acar, MA Guler, B Gerceker, et al. Multi-objective crashworthiness optimization of tapered thin-walled tubes with axisymmetric indentations. Thin Wall Struct. 49:2011;94–105.

[25] , LS-DYNA keyword user's manual, version 970 J.O, Hallquis., 2003. Livermore Software Corporation, California.

[26] Offset deformable barrier frontal impact testing protocol, version 7.1. European New Car Assessment Programme (Euro NCAP), Brussels; 2015.

[27] B Wang, G Lu. Mushrooming of circular tubes under dynamic axial loading. Thin Wall Struct. 40:2002;167–182.

[28] G Lu, T Yu. Energy absorption of structures and materials, Woodhead Publishing Ltd.; 2003., Cambridge

[29] AG Mamalis, DE Manolakos, MB Ioannidis, et al. Finite element simulation of the axial collapse of thin-wall square frusta. Int J Crashworthiness. 6:2001;155–164.